Ground State Polarized Photofragments Study by Using Resonance and Off-Resonance Probe Beam Techniques

B. V. Picheyev,* A. G. Smolin, and O. S. Vasyutinskii*

Ioffe Institute, Russian Academy of Sciences, 194021 St. Petersburg, Russia

Received: April 15, 1997; In Final Form: July 21, 1997[⊗]

The optical magnetic birefringence (Faraday) technique that can be used to study the anisotropy distributions of the angular momenta of photofragments produced in molecular photodissociation is compared theoretically and experimentally with the magnetic dichroism technique. The frame independent tensor form of the general expression describing the difference between an initial and a final polarization matrix of a probe light beam passing through the photofragment vapor is presented and analyzed. The procedure of detection of the photofragment electron orientation and alignment angular distributions by Doppler spectroscopy using each of the techniques is studied theoretically. The angular independent anisotropy orientation and alignment parameters describing photodissociation dynamics that can be determined from these studies are presented. It is shown that in principle each of the techniques can give the same information about the photodissociation dynamics; however, the birefringence technique has an undeniable advantage since it leads to an increase in accuracy of the experimental data. Both magnetic birefringence and magnetic dichroism techniques were used experimentally to study the spin orientation of ground state Rb atoms produced in photodissociation of RbI at 266 nm by circularly polarized laser light. The experiment was not of the Doppler spectroscopy type, but use of different ^{85}Rb and ^{87}Rb isotopes in the dissociation cell and in the probe light source allows detection of the oriented atomic photofragments separately by each of the techniques. Obtained experimental results are in agreement with the theoretical predictions. Contribution of the orientation of the Rb hyperfine structure energy states to the observed signals were also studied and treated theoretically. The initial degree of the electron spin orientation of the Rb atoms produced in the reaction was found to be $P_e = 0.11 \pm 0.02$.

I. Introduction

Vector correlations in molecular photodissociation have lately attracted considerable interest since they can provide very detailed and important information about the dynamics of half-collision processes.[1] Several types of the correlations have been under study. One of these is a correlation between the polarization vector **e** of the dissociation light and the recoil direction **k** of the fragments that gives rise to the anisotropic angular distributions of the photofragments in space.[2] Another correlation occurs between the vector **e** and the distribution among the relative population of magnetic sublevels *m* corresponding to the projection of the angular momentum *j* of a photofragment on the space-fixed *Z* axis resulting in anisotropic distributions of the vectors *j* in space.[3] Usually these distributions can be described by their three main polarization momenta: population (*m* independent), orientation (*m* selection), and alignment (|*m*| selection). Population is proportional to the total population of the magnetic sublevels, orientation is proportional to the mean magnetic dipole momentum of the fragments ensemble, and alignment is proportional to the mean quadrupole momentum of the fragments ensemble.[4] Other and more complicated types of correlations have also been under study and can lead to higher order polarization moments of the photofragments.[5] It has been shown[6] that investigations of the photofragment polarization moments can provide detailed and important information about photodissociation dynamics, including the symmetry and shape of excited molecular surfaces, knowledge about reaction channels, nonadiabatic interactions, interference effects, and more.

Investigations of polarized nonfluorescing photofragments have usually employed polarized laser photolysis combined with detection-polarized laser-probing techniques to characterize the anisotropy of the reaction products. Several different detection techniques including one-photon and multiphoton laser-induced fluorescence (LIF) techniques, the resonance enhanced multiphoton ionization (REMPI) technique, and the ion imaging technique have been suggested and used.[7,8] An experimental technique consisting of measurement of the output polarization of a probe light that is in resonance with the photofragment absorption line was employed in our group to study polarized alkali and thallium atoms.[9] In order to discriminate orientation and alignment of the atomic fragments from background, we modulated them by applying a small external magnetic field and thus obtained sensitivity that is comparable with that provided by the one-photon LIF technique. An important advantage of one-photon detection schemes compare to multiphoton schemes is in their relative facility in extracting dynamical information from the experimental data because corresponding theoretical expressions are simpler.

The detection techniques mentioned above explore magnetic optical dichroism of the photofragment vapor and result in real optical transitions from the fragment states under study. A disadvantage of this detection technique is that the interaction between the probe light and the fragments can saturate the transition and thus perturb the initial distribution among the relative population of magnetic sublevels. Usually the small polarization signal under study has to be detected in the presence of a large absorption signal coming from the unpolarized part of the photofragments. Moreover, the concentration of produced photofragments for the resonance techniques should be kept at sufficiently a low level to prevent effects of thick optical layer for the probe light (see, e.g., ref 9). All these effects can reduce the experimentally achieved signal-to-noise ratio and sophisticate much the experimental situation.

* Corresponding authors.

[⊗] Abstract published in *Advance ACS Abstracts,* October 1, 1997.

S1089-5639(97)01287-5 CCC: $14.00

An alternative for the resonance detection schemes of polarized photofragments is the paramagnetic Faraday rotation technique that explores the photofragment magnetic optical birefringence of the vapor and is based on the fact that the gyrotropic component of the atomic/molecular polarisability causes the electric field of the probe off-resonant light wave to be rotated by a certain angle after the light passed through polarized vapor. The effect is known from optical pumping experiments;[10,11] its theoretical treatment based on the density matrix formalism was done for the case of thin optical layer by Laloë and Cohen-Tannoudji[12] and generalized for the case of thick optical layer by Kupriyanov et al.[13] The paramagnetic Faraday rotation technique found important application in molecular and solid state spectroscopy[14] but was never used to detect and analyze polarized photofragments.

The purpose of this work is to study theoretically how the paramagnetic Faraday rotation technique can be used in photodissociation experiments, to detect experimentally polarized atomic photofragments using this technique and to compare the experimental results obtained on the same atoms using resonance and off-sequence detection schemes. Only one-photon absorption schemes are under study. The irreducible components of the density matrices (state multipoles representation)[4] are used throughout the paper both for the light and for the photofragment ensembles. It is shown that application of the paramagnetic Faraday rotation technique to the field of molecular photodissociation can be very hopeful because it provides an investigator with a relatively simple, nonperturbing detection technique that is quite compatible with a VUV laser as a probe beam source.

The organization of the paper is as follows. In section II general theoretical expressions for the density matrix of a probe light passed through polarized atomic vapor are transformed to a frame-independent state multipoles representation and then analyzed. Necessary conditions to determine absorption and dispersion cross sections containing information about photodissociation dynamics are studied. In section III the particular cases of detection procedure are described. There are presented and discussed expressions for absorption cross sections and orientation and alignment cross sections in the case of direct photodissociation both for resonant and off-resonant detection schemes. In section IV the results of experimental studies of spin-oriented Rb atoms produced in photodissociation of RbI molecules by circularly polarized light are presented. The detection of the oriented Rb atoms were provided in both resonance and off-resonance schemes as a function of RbI concentration. The initial degree of orientation of the Rb atoms was also determined. The results obtained by both techniques are compared and discussed.

II. General Expressions for Probe Light Density Matrix in State Multipoles Representation

2.1. Definitions. We describe an arbitrarily polarized probe light with initial intensity I_0 passing successively through an optically active photofragments vapor and an analyzer and then falling on a detector as it is shown in Figure 1. In the following the atomic vapor will be discussed, but the obtained results will be also valid for paramagnetic molecular vapor. We will be interested in the polarization and intensity I of the output light. The photofragments are assumed to have ground and excited states total angular momenta j_g and j_e and their Z projections μ and m respectively and described by the density matrix elements $\rho^{j_g}_{\mu\mu'}$, and $\rho^{j_e}_{mm'}$. The off-diagonal over the j_g, j_e values density matrix elements can be neglected in the low-intensity light approximation that is used in this paper. The irreducible components of the ground state density matrix (state multipoles)

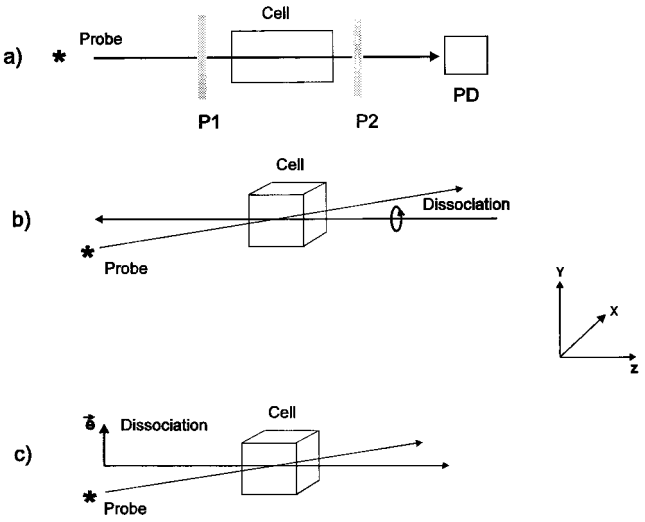

Figure 1. Experimental geometries. (1) General geometry of the probe light propagating through the absorption cell. (2) Geometry of production and detection of the photofragments orientation. The dissociation light is circularly polarized and directed under the small angle to the Z axis. The probe light beam propagates through the cell along Z axis. (3) Geometry of production and detection of the photofragments alignment. The dissociation light is linearly polarized along Y axis. The probe light beam propagates through the cell along the Z axis.

are defined as follows:[4,11]

$$\rho^{j_g}{}_{KQ} = \mathrm{Tr}[\hat{\rho}^{j_g}\hat{T}_{KQ}(j_g j_g)] \tag{1}$$

The irreducible components of the excited state density matrix are defined in a like manner. The operator $T_{KQ}(jj)$ in (1) is an irreducible tensor:

$$\hat{T}_{KQ}(j_g j_g) = \sum_{\mu,\mu'} \frac{\Pi_K}{\Pi_{j_g}} C^{j_g\mu'}_{j_g\mu KQ} |j_g\mu'\rangle\langle j_g\mu|$$

where $C^{j_g\mu'}_{j_g\mu KQ}$ are Clebsch−Gordan coefficients, K is a rank of the tensor operator, and Q is its component along the Z axis. The symbol $\Pi_{XY...}$ here and everywhere below denotes $\Pi_{XY...} = [(2X + 1)(2Y + 1)...]^{1/2}$. The density matrix component in (1) relating to $K = 0$ is proportional to the total population of the Zeeman atomic sublevel, while the components relating to $K = 1$ and $K = 2$ (orientation and alignment) are proportional to the cyclic components of the mean dipole angular momentum $\langle j^{(1)}{}_Q\rangle$ and to quadrupole angular momentum $\langle j^{(2)}{}_Q\rangle$ of the atomic ensemble, relatively.[4]

The polarization matrix of the monochromatic light propagating along the Z axis can be introduced as follows[15]

$$\pi = \begin{pmatrix} \langle \epsilon_X \epsilon_X^* \rangle & \langle \epsilon_X \epsilon_Y^* \rangle \\ \langle \epsilon_Y \epsilon_X^* \rangle & \langle \epsilon_Y \epsilon_Y^* \rangle \end{pmatrix} \tag{2}$$

where ϵ_X, ϵ_Y are amplitudes of the electric field Cartesian components of the light and angular brackets denote time averaging. The intensity of the light I obeys usual expression $I = \mathrm{Tr}(\pi)$. Using standard cyclic components of the electric field vector:

$$\epsilon_0 = \epsilon_Z, \quad \epsilon_{\pm 1} = \mp\frac{\epsilon_X \pm i\epsilon_Y}{\sqrt{2}}$$

the matrix π can be written in the cyclic basis:

$$\pi_{q_1q_2} = \langle \epsilon_{-q_1} \epsilon^*_{-q_2} \rangle; \quad q_1,q_2 = \pm 1 \tag{3}$$

The matrix π in (2) can be also rewritten in the following form

$$\pi = \frac{I}{2}\begin{pmatrix} 1 + S_1 & S_2 - iS_3 \\ S_2 + iS_3 & 1 - S_1 \end{pmatrix} \tag{4}$$

where S_1, S_2, and S_3 are Stokes parameters of the light.[15] The particular cases (a) $S_1 = +1/-1$, $S_2 = 0$, $S_3 = 0$; (b) $S_1 = 0$, $S_2 = +1/-1$, $S_3 = 0$; (c) $S_1 = 0$, $S_2 = 0$, $S_3 = +1/-1$ correspond to (a) the light is linearly polarized along *X*/*Y* axes; (b) the light is linearly polarized on the 45°/135° angle to the *X* axis; (c) the light is right/left-hand circularly polarized, respectively. The Stokes parameters are very important because they can easily be measured experimentally.

The irreducible components of the light polarization matrix in (2), (3) are defined as follows:[4,11]

$$\Phi_{KQ} = \frac{1}{I}\sum_{q_1q_2}(-1)^{1+q_1} C^{KQ}_{1q_1 1q_2} \langle \epsilon^*_{-q_1} \epsilon_{q_2} \rangle = \frac{1}{I}\sum_{q_1q_2}(-1)^{1+K+q_2} C^{KQ}_{1-q_1 1q_2} \langle \epsilon_{-q_1} \epsilon^*_{-q_2} \rangle \tag{5}$$

Due to the symmetry properties of the Clebsch−Gordan coefficients, the index K in (5) is limited to the values $K = 0$, 1, 2, and the Φ_{KQ} matrix elements corresponding to (4) can be expressed in terms of the light Stokes parameters as follows:

$$\Phi_{00} = \frac{1}{\sqrt{3}}; \quad \Phi_{10} = \frac{S_3}{\sqrt{2}}; \quad \Phi_{20} = \frac{1}{\sqrt{6}}; \quad \Phi_{22} + \Phi_{2\text{-}2} = -S_1; \quad \Phi_{22} - \Phi_{2-2} = -iS_2 \tag{6}$$

The definition in (5) is not restricted to the case q_1, $q_2 = \pm 1$ described above when the light propagates in the Z direction but can also be used for an arbitrary direction of light propagation and polarization. The expressions for the components of the density matrix Φ_{KQ} for some particular cases are given in refs 6e and 17.

Application of the irreducible density matrix representation both for the light and for the photofragments has an undeniable advantage because it allows one to write frame independent tensor equations for experimentally measured quantities, to more easy solve these equations and analyze the obtained results.

2.2. Polarization of the Resonant and Off-Resonant Light Passed through Optically Active Vapor. Following the results of Cohen−Tannoudji and Laloë[12] a general expression describing the difference between the initial π_I and the final π polarization matrices in (2) of monochromatic light passed through polarized photofragment vapor along the Z axis in the first order on the light intensity and on the optical thickness of the vapor can be written as follows:

$$\pi - \pi_I = -[G_A, \pi_I]_+ - i[G_D, \pi_I] \tag{7}$$

where [...] and $[...]_+$ are the commutator and anticommutator, respectively. The functions G_A and G_D describe absorption and dispersion properties of the vapor. The function G_A is Hermitian, while the function G_D is anti-Hermitian. When the atomic density is homogeneous within the vapor length l, the functions G_A and G_D can be written as follows

$$G_A = \frac{1}{2}(G + G^+); \quad G_D = \frac{1}{2}(G - G^+) \tag{8}$$

$$G \equiv [G_\omega(t)]_{ij} = \frac{2\pi N\omega l}{\hbar c}\int \mathrm{d}^3\,\mathbf{v}\,\frac{\mathrm{Tr}[\rho^{j_g}(\mathbf{v},t),[(\mathbf{e}_i^*\mathbf{d})(\mathbf{e}_j\mathbf{d})]]}{-i(\omega - \omega_0 - \mathbf{kv}) + \Gamma/2}$$

where ω is the light frequency, ω_0 is an atomic transition resonance frequency, N is the atomic concentration, $\mathbf{e}_i$ is a light polarization unit vector, $\mathbf{d}$ is a photofragment optical transition electric dipole moment, $\mathbf{v}$ is a relative photofragment recoil velocity, $\mathbf{k}$ is a light wave vector, and Γ is a natural rate of spontaneous decay of the photofragment excited state.

Writing the expression (8) we assume that the photofragment density matrix elements $\rho^{j_g}_{\mu,\mu'}(\mathbf{v},t)$ with different Z-projections μ, μ' of the angular momentum j_g have different $\mathbf{v}$-dependencies according to the recent theoretical and experimental results.[5] The state multipole representation for both photofragment and light density matrices ((1) and (5)) can be used to transform (7) and (8) to the tensor form. By combining (7) and (8) and applying the transformations (1) and (5) it is found after using the properties of $3-j$ and $6-j$ symbols[16] that the difference between the initial and final light polarization matrices can be written as:

$$I(\omega)\Phi_{KQ} - I_0\Phi^0_{KQ} = (-1)^{j_g+j_e+K} 3I_0 Nl \sum_{K_0,k} \Pi_{K_0 k j_g} \begin{Bmatrix} k & 1 & 1 \\ j_e & j_g & j_g \end{Bmatrix} \begin{Bmatrix} K_0 & k & K \\ 1 & 1 & 1 \end{Bmatrix} [L_A[\Phi^0_{K_0} \otimes A_k(\omega)]_{KQ} + iL_D[\Phi^0_{K_0} \otimes D_k(\omega)]_{KQ}] \tag{9}$$

where $L_A = [1 + (-1)^{K+K_0+k}]/2$; $L_D = [1 - (-1)^{K+K_0+k}]/2$, the terms $[\Phi^0_{K_0} \otimes A_k(\omega)]_{KQ}$, $[\Phi^0_{K_0} \otimes D_k(\omega)]_{KQ}$ in (9) denote tensor products,[16] and $A_{kq}(\omega)$ and $D_{kq}(\omega)$ are irreducible absorption and dispersion cross sections respectively:

$$[\Phi^0_{K_0} \otimes A_k(\omega)]_{KQ} = \sum_{Q_0,q} C^{KQ}_{K_0Q_0kq}\, \Phi^0_{K_0Q_0} A_{kq}(\omega)$$

$$A_{kq}(\omega) = C\int \mathrm{d}^3\,\mathbf{v}\,\frac{\rho^{j_g}_{kq}(\mathbf{v})\Gamma/2}{(\omega - \omega_0 - \mathbf{kv})^2 + \frac{\Gamma^2}{4}} \tag{10}$$

$$D_{kq}(\omega) = C\int \mathrm{d}^3\,\mathbf{v}\,\frac{\rho^{j_g}_{kq}(\mathbf{v})\cdot(\omega - \omega_0 - \mathbf{kv})}{(\omega - \omega_0 - \mathbf{kv})^2 + \frac{\Gamma^2}{4}} \tag{11}$$

$$C = \frac{4\pi\omega|\langle j_g||d||j_e\rangle|^2}{3\hbar c\Pi_{j_g}}$$

The irreducible tensors Φ^0_{KQ} and Φ_{KQ} in (9) are initial and residual light polarization matrices. The indices K_0, Q_0 and K, Q relate to the initial and residual light polarization, respectively, while the indices k, q relate to the photofragment polarization, all the indices being integer.

The general expressions (9)−(11) describe the change of the probe light polarization matrices due to absorption and dispersion properties of the atomic vapor. The term containing the absorption cross section $A_{kq}(\omega)$ in (9) describes the influence of magnetic optical dichroism of the photofragment vapor on the transmitted light polarization. According to (9) this effect can occur only if the sum of the indices K, K_0 and k are *even* numbers because only in this case does the coefficient L_A differ from zero. The term containing the dispersion cross section $D_{kq}(\omega)$ describes the influence of the magnetic optical birefringence of the photofragment vapor on the transmitted light polarization. This effect can occur only if the sum of the indices

K, K_0, and k are *odd* numbers because only in this case the coefficient L_D in (9) differs from zero. The irreducible cross sections $A_{kq}(\omega)$ and $D_{kq}(\omega)$ ((10) and (11)) are experimentally measured quantities that can be used to obtain the photofragment density matrix elements $\rho_q^{j_g}(\mathbf{v})$, which contain all information about the photodissociation dynamics.[5c]

Applying (9)−(11) to analyze the photofragments' polarization, one should have in mind that in any choice of laboratory frame the full set of cross section components (10), (11) corresponding to all possible projections q, (i.e. $q = 0, \pm1$ for $k = 1$ and $q = 0, \pm1, \pm2$ for $k = 2$) must be expected to contribute simultaneously under most experimental conditions; moreover, each of these cross sections will have a specific dependence on the probe light frequency ω. These are the results of intrinsic correlations in the decaying molecules.[5] This property of the photodissociation process complicates interpretation of experimental results compared to typical conditions of optical pumping experiments[11] where an appropriate choice of laboratory frame can significantly reduce the number of the atomic density matrix elements. It will be shown later that the full number of independent anisotropy parameters that is necessary to describe the angular dependence of photofragment orientation and alignment produced in direct photodissociation is equal to seven (three for the orientation and four for the alignment). Another peculiar property of the photodissociation experiment is that the absorption and dispersion profiles (10) and (11) are usually not of the Gaussian type shape and depend on the photodissociation dynamics.

In the next section (9)−(11) will be used to describe the procedures used to detect of photofragment's polarization momenta using some typical experimental geometries, and resonant detection schemes will be compared with off-resonant ones.

III. Particular Cases of the Detection Procedure

3.1. No Analyzer in Front of the Photodetector: Orientation and Alignment Detection. We will describe the general case of the photodissociation experiment and assume that the following photofragment irreducible density matrix elements differ from zero

$$\rho_{00}^{j_g},\ \rho_{10}^{j_g},\ \rho_{1\pm1}^{j_g},\ \rho_{20}^{j_g},\ \rho_{2\pm1}^{j_g},\ \rho_{2\pm2}^{j_g} \tag{12}$$

where $\rho_{kq}^{j_g} = (-1)^q(\rho_{k-q}^{j_g})^*$.[4] The density matrix elements (12) are assumed to be functions of the recoil velocity $\mathbf{v}$ and the corresponding cross sections (10), (11) are assumed to differ from zero. The alignment $\rho_{2q}^{j_g}$ can be produced, for instance, if linearly polarized photodissociation light is used, while both orientation and alignment, $\rho_{1q}^{j_g}$, $\rho_{2q}^{j_g}$, can be produced with circularly polarized photodissociation light (see, e.g., ref 4). Orientation and alignment parameters P_0, A_0 can be constructed by combining the matrix elements (12) in the usual way.[18] Now we analyze some particular cases of (9) and the possibility of separate experimental determination of the cross section elements (10), (11).

We first consider the experimental geometry where there is no polarization analyzer P_2 in front of the photodetector (see Figure 1) and thus full residual light intensity $I(\omega)$ is detected. This experimental geometry was recently used, for instance, by North and Hall[1h] in their vector correlation studies of NCCN photodissociation. Using the condition K, $Q = 0$ in (9), one can obtain that due to the symmetry properties of the Clebsch-Gordan coefficients the other indices must obey the conditions $K_0 = k$; $Q_0 = -q$. Using (5) it can be shown that the photofragment orientation ($k = 1$) can be detected only by using circularly polarized probe light, while the photofragment alignment ($k = 2$) can be detected by using either arbitrarily polarized or unpolarized light. Only the absorption cross sections A_{kq} (10) give a contribution to the signal (here and further we omit the argument ω in all expressions for brevity). Using (6) and properties of the $3-j$ and $6-j$ coefficients[16] (9) can be transformed to

$$I - I_0 = (-1)^{j_g+j_e}\, 3I_0 Nl\pi_{j_g}\sum_{K_0}\begin{Bmatrix} K_0 & 1 & 1 \\ j_e & j_g & j_g \end{Bmatrix}(\Phi_{K_0}^0 \cdot A_{K_0}) \tag{13}$$

where the term $(\Phi_{K_0}^0 \cdot A_{K_0})$ denotes the scalar product:

$$(\Phi_{K_0}^0 \cdot A_{K_0}) = \sum_{Q_0}(-1)^{Q_0}\Phi_{K_0Q_0}^0 A_{K_0-Q_0}$$

The expression (13) describes absorption of the monochromatic probe light by arbitrarily polarized photofragments. All cross section elements (10) can be in principle determined by varying direction and polarization of the probe light. The same type of expression describes, under some restrictions, the one-photon LIF signal and the $1 + n$ photon REMPI signal. In the limiting case $(\mathbf{kv})^2 \gg \Gamma^2/4$ that is routine for the direct dissociation process and for a sharp photofragment velocity distribution the integral over $\mathbf{v}$ in (10) can be easily evaluated. If then one writes (13) in the light frame, it becomes analogous to the well-known expression for the absorption intensity in the polarized Doppler spectroscopy theory (see, e.g. (1) in ref 7f).

3.2. Detection of the Photofragment Orientation with the Analyzer in Front of the Photodetector. Second, we consider the experimental geometry where the analyzer P_2 in front of the photodetector (see Figure 1) selects the polarization of the transmitted light. This experimental geometry was used to study oriented and aligned Tl($^2P_{3/2}$) and oriented Rb($^2S_{1/2}$) photofragments in ref 9 and will be analyzed in two following sections in more detail. Determination of photofragment orientation and alignment cross-sections will be described using resonance and off-resonance detection techniques separately.

If photofragment's orientation $\rho_{1q}^{j_g}$ is determined by the resonance detection technique, either the $K_0 = 1$ or $K = 1$ component of the light polarization matrix must differ from zero (see (9)). Let the initially unpolarized probe light beam be directed along the Z axis. Then the initial light polarization matrix elements are as follows:

$$\Phi_{00}^0 = 1/\sqrt{3},\quad \Phi_{1Q}^0 = 0,\quad \Phi_{20}^0 = 1/\sqrt{6},\quad \Phi_{2\pm1}^0 = 0,\quad \Phi_{2\pm2}^0 = 0 \tag{14}$$

Magnetic circular dichroism of the photofragment vapor results in partial circular polarization of the transmitted light that can be determined by the circular analyzer (P_2 in Figure 1) in front of the photodetector. Substituting (14) into (9) and combining (2)−(5), the expression for the Stokes parameter S_3 in (4) of the transmitted light can be written using (6) as

$$S_3 = \frac{I_+ - I_-}{I_+ + I_-} = (-1)^{j_g+j_e} 3\Pi_{j_g} Nl\begin{Bmatrix} 1 & 1 & 1 \\ j_e & j_g & j_g \end{Bmatrix}\frac{A_{10}}{\sqrt{2}}\frac{I_0}{I} \tag{15}$$

where I_+,I_- are intensities of right- and left-hand circularly polarized output light respectvely. The intensity I in (15) can be obtained from (13) and (14):

$$I = I_0\left[1 - Nl\left(A_{00} - (-1)^{j_g+j_e} 3\Pi_{j_g}\begin{Bmatrix} 2 & 1 & 1 \\ j_e & j_g & j_g \end{Bmatrix}\frac{A_{20}}{\sqrt{6}}\right)\right] \tag{16}$$

It can be seen from (15) that probe light propagating along the *Z* axis together with a circular polarization analyzer in front of the photodetector can be used to determine the longitudinal cross section A_{10} but is not sensitive to the transverse cross section $A_{1\pm1}$. The latter can be determined using the light propagating perpendicularly to the *Z* axis.

If the photofragment's orientation is determined by the off-resonance detection technique, the sum of the K_0 and K light matrix ranks must be even. The initial probe light can be linearly polarized and propagate in the *Z* direction. Magnetic optical birefringence of the vapor results in rotation of the light polarization vector **e** by an angle θ that can be determined by a linear analyzer in front of the photodetector. Assuming the initial polarization vector of the light to be parallel to the *Y* axis, the relationship between the Stokes parameter S_2 of the residual light and the angle θ can be written as $S_2 = \sin 2\theta$. The polarization matrix elements of the initial light are as follows:

$$\Phi^0_{00} = 1/\sqrt{3}, \quad \Phi^0_{1Q} = 0, \quad \Phi^0_{20} = 1/\sqrt{6}, \quad \Phi^0_{2\pm1} = 0, \quad \Phi^0_{2\pm2} = 1/2 \quad (17)$$

By combining (2), (5), (6), (9), and (17), the Stokes parameter S_2 of the transmitted light can be written as

$$S_2 = \frac{I_{45} - I_{-45}}{I_{45} + I_{-45}} = (-1)^{j_g+j_e} 3\Pi_{j_g} Nl \begin{Bmatrix} 1 & 1 & 1 \\ j_e & j_g & j_g \end{Bmatrix} \frac{D_{10}}{\sqrt{2}} \frac{I_0}{I} \quad (18)$$

where I_{45}, I_{-45} are intensities of the residual light linearly polarized on $\pm45°$ to the *Y* axis, respectively. Note that (18) has the same form as the (15) if one changes the dispersion cross section D_{10} to the absorption one and that the light propagating along the *Z* axis is sensitive to the longitudinal ($q = 0$) component of the orientation cross section only.

3.3. Detection of the Photofragment Alignment with the Analyzer in Front of the Photodetector. If photofragment alignment $\rho^{j_g}_{2q}$ is determined by the resonance detection technique, the sum of the K_0 and K matrix ranks must be even (see (9)). Let the initially unpolarized probe light beam propagate along the *Z* axis as in ref 9. Then the magnetic linear dichroism of the photofragment vapor results in partial linear polarization of the transmitted light that can be determined by a linear analyzer in front of the photodetector. The polarization matrix elements of the initial light are shown in (14).

Substituting (14) into (9), the expressions for the residual light matrix elements $\Phi_{2\pm2}$ can be obtained. Then the degree of linear polarization of the transmitted light can be written as

$$S_1 = \frac{I_X - I_Y}{I_X + I_Y} = (-1)^{j_g+j_e+1} 3\Pi_{j_g} Nl \begin{Bmatrix} 2 & 1 & 1 \\ j_e & j_g & j_g \end{Bmatrix} \frac{I_0}{I} \mathrm{Re}(A_{22}) \quad (19)$$

where I_X,I_Y are intensities of the residual light linearly polarized along the *X* and *Y* axes, respectively. It can be seen from (19) that determination of the Stokes parameters S_1 can be used to study the transverse component of the alignment cross section A_{22} and that the procedure is not sensitive to other cross sections A_{20}, A_{21}.

If photofragment alignment is determined by the off-resonance detection technique, either the $K_0 = 1$ or $K = 1$ component of the light polarization matrix must differ from zero, and therefore either the initial light must be circularly polarized or the analyzer in front of the photodetector must be a circular one. Let us describe the experimental geometry where the initial probe light beam is circularly polarized and propagates along the *Z* axis. The polarization matrix elements of the initial light are as follows:

$$\Phi^0_{00} = 1/\sqrt{3}, \quad \Phi^0_{10} = 1/\sqrt{2}, \quad \Phi^0_{1\pm1} = 0, \quad \Phi^0_{20} = 1/\sqrt{6}, \quad \Phi^0_{2\pm1} = 0, \quad \Phi^0_{2\pm2} = 0 \quad (20)$$

The optical birefringence of the vapor changes the initial circular polarization of the light to elliptical polarization with general axes directed on the $\pm45°$ to the alignment axis that can be detected measuring the Stokes parameter S_2 of the light by using a linear analyzer. Substituting (20) into (9), the expressions for the residual light matrix elements $\Phi_{2\pm2}$ can be obtained. Then the Stokes parameter S_2 of the transmitted light can be written as

$$S_2 = \frac{I_{45} - I_{-45}}{I_{45} + I_{-45}} = (-1)^{j_g+j_e+1} 3\Pi_{j_g} Nl \begin{Bmatrix} 2 & 1 & 1 \\ j_e & j_g & j_g \end{Bmatrix} \frac{I_0}{I} \mathrm{Re}(D_{22}) \quad (21)$$

It is seen again that the described experimental geometry is sensitive only to the transverse alignment elements D_{22} and that the only difference between (19) and (21) is that the former contains the absorption while the latter the dispersion cross section. The expressions (15), (18), (19), and (21) describe the results of application of resonance and off-resonance techniques to measure orientation and alignment photodissociation cross sections.

It should also be noted that the expression for the light intensity I (16) contains the population and alignment cross sections A_{00}, A_{20} that are also to be determined from the experiment. The terms containing these cross sections (or the second one only) can be neglected in (16) compared to unity if total absorption of the light by the photofragments, or their alignment, is small. It can be shown using (4) and (9) that all cross sections can be determined as a function of frequency ω combining the results of several experiments when the light propagates through the vapor in different directions.

If the probe light is not monochromatic, (10), (11) should be integrated over the frequency ω using a spectral profile of the incident light $I_0 = I_0(\omega)$. If the spectral width of the profile $I_0(\omega)$ is larger that the spectral width of the photofragment absorption cross section (10) the integral over ω can be written in the form:

$$\bar{A}_{kq} = \int A_{kq}(\omega)\, I_0(\omega)\, \mathrm{d}\omega \approx C\, J^A \langle \rho^{j_g}_{kq} \rangle \quad (22)$$

where $J^A = \pi I_0(\omega_0)$ and the angular brackets mean averaging over the recoil angles. The averaged expression for the dispersion cross section (11) can also be simplified in the case of large detunings $|\omega - \omega_0| \gg |\mathbf{kv}|$ and can be written as

$$\bar{D}_{kq} = \int D_{kq}(\omega)\, I_0(\omega)\, \mathrm{d}\omega \approx C\, J^D \langle \rho^{j_g}_{kq} \rangle \quad (23)$$

where

$$J^D = \int \frac{I_0(\omega)}{(\omega - \omega_0)}\, \mathrm{d}\omega$$

The expressions (13), (15), (18), (19), and (21) containing the cross sections (10) and (11) presented above are general and do not depend on where the polarized photofragments come from. The explicit forms of the absorption and dispersion cross sections (10), (11) differ from each other for different types of the photoprocesses according to the photofragment density matrix angular dependence. The widely used way to treat the

vector correlation phenomenon is to expend the photofragment density matrix over the bipolar harmonics and then determine the bipolar moments $b_Q^K(k,S)$ that contain the information about the dissociation dynamics.[5a,7f] However in the next section of this article we use another approach presenting the explicit angular dependence of the photofragment density matrix $\rho_{kq}^j(\vartheta,\varphi)$ from the detailed quantum mechanical theory[5c] in terms of orientation and alignment *anisotropy parameters*. Only the case of direct photodissociation within the condition of validity of axial recoil approximation will be discussed. The advantage of this approach is that the anisotropy parameters have clear physical meaning and relate directly to the different photodissociation mechanisms.

3.4. Absorption and Dispersion Cross Sections V-Dependencies. In some interval of the relative recoil impulses p the photofragment density matrix elements can be presented in the form

$$\rho_{kq}^j(\mathbf{p}) = (2\pi\hbar)^3 f(p)\frac{\sigma_{kq}^j(\varphi,\vartheta)}{\Pi_j \bar{\sigma}_{00}} \tag{24}$$

where $\sigma_{kq}^j(\varphi,\vartheta)$ is a differential cross section for one-photon fragmentation of a molecule to a fragment with total electron momentum j, φ and ϑ are photodissociation recoil polar angles; $\mathbf{p}$ is a relative photofragment recoil impulse, $\bar{\sigma}_{00}$ is the zero-rank excitation matrix integrated over total recoil solid angle, and $f(p)$ is a photofragment distribution over the modulus of their relative recoil impulse p that can be approximated by a Gaussian function centered at $p = p_0$[13]

$$f(p) \approx \frac{1}{p_0^2\sqrt{2\pi s_0^2}}\, e^{-(p-p_0)^2/2s_0^2} \tag{25}$$

where the parameter s_0^2 is related to the width of the parent molecules Bolzmann impulse distribution. The absorption and dispersion cross sections (10) and (11) are calculated and presented below for several particular cases as functions of the light frequency ω. The light was supposed to propagate along the Z axis. The cross sections were calculated using the following values of the parameters Γ, $k\upsilon_0$, s_0^2 related to the detection of polarized ground state Rb atoms produced in photodissociation of RbI at 266 nm in bulk conditions that were experimentally studied in this work: $\Gamma \approx 36$ MHz, $k\upsilon_0 \approx 7600$ MHz, $(p_0/s_0)^2 \approx 10$.

3.4.1. Zeroth-Order Cross Sections. The differential cross section of the zero-order for one-photon fragmentation can be written in the following famous form[2]

$$\sigma_{00}^j(\varphi,\vartheta) = \frac{\sigma_0}{4\pi}[1 + \beta_0 P_2(\cos\vartheta)] \tag{26}$$

where β_0 is anisotropy parameter.

If circularly polarized or unpolarized dissociation light propagates in the Z direction for pure parallel transitions, β_0 stands for the limiting value $\beta_0 = -1$ that gives $\sim\sin^2\vartheta$ angular distribution while for pure perpendicular transitions β_0 stands for $\beta_0 = {}^1/_2$ that gives $\sim(1 + \cos^2\vartheta)$ angular distribution. If linearly polarized along the Z axis light, for pure parallel transitions β_0 stands for the value $\beta_0 = 2$ that gives $\sim\cos^2\vartheta$ angular distribution while for pure perpendicular transitions β_0 stands for $\beta_0 = -1$ that gives $\sim\sin^2\vartheta$ angular distribution. The corresponding well-known[1,2] absorption cross sections A_{00} are shown in Figure 2 as function of the relative frequency detuning $x = (\omega - \omega_0)/k\upsilon_0$. Only absorption zeroth-order cross sections (10) differ from zero.

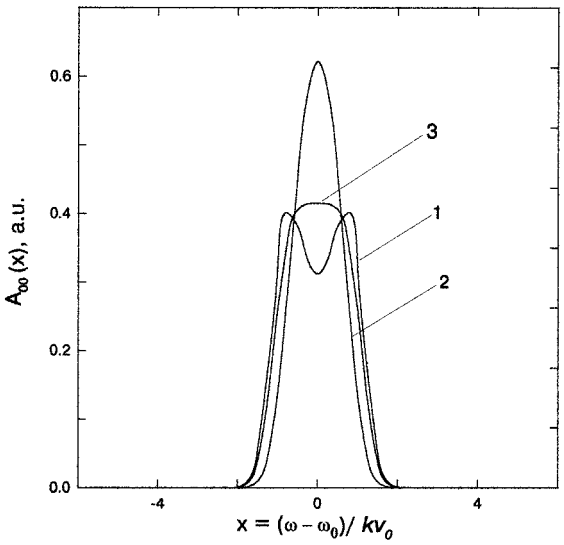

Figure 2. Absorption cross sections A_{00} versus relative probe laser frequency detuning x. (1) The photofragments produced via pure perpendicular optical transitions in the dissociating molecules ($\beta_0 = {}^1/_2$). (2) The photofragments produced via pure parallel optical transitions in the dissociating molecules ($\beta_0 = 1$). (3) Isotropic case ($\beta_0 = 0$).

3.4.2. First-Order (Orientation) Cross Sections. As shown in (10), (11), (15), and (18), both resonance and off-resonance orientation detection schemes where the probe light beam propagates along the Z axis lead to signals that depend on the diagonal orientation cross section σ_{10}^j, where j is the total photofragment angular momentum. According to the results of the ref 5c, the components of the differential orientation cross section $\sigma_{1q}^j(\varphi,\vartheta)$ can be described by three anisotropy parameters that are independent of the angles φ, ϑ and from each other. These parameters can be defined as follows

$$\alpha_1 = \frac{f_1(1,1)}{f_0(0,0) + 2f_0(1,1)} \tag{27a}$$

$$\gamma_1 = \frac{2\mathrm{Re}[f_1(1,0)]}{f_0(0,0) + 2f_0(1,1)} \tag{27b}$$

$$\gamma_1' = \frac{2\mathrm{Im}[f_1(1,0)]}{f_0(0,0) + 2f_0(1,1)} \tag{27c}$$

where $f_K(q,q')$ are photodissociation *dynamical functions*.[5c,6d,e] The dynamical functions are a result of the detailed quantum mechanical treatment and contain all the information of the transition dipole moments and fragmentation dynamics. In the high-j limit approximation (semiclassical limit), these functions can be presented as linear combinations of the well-known bipolar moments[5a] (see Appendix). The "diagonal" dynamical functions for which $q = q'$ are real, while the "off-diagonal" functions for which $q \neq q'$ can be complex. The first anisotropy parameter α_1 describes the orientation of the photofragments coming from an incoherent pure perpendicular optical transition in the dissociating molecule, while two others describe the orientation of the photofragments coming from coherent superposition of a parallel and a perpendicular transition.

We will study the experimental geometry shown in Figure 1b when dissociation and probe beams propagate at a small angle to each other in opposite directions along the Z axis. For left-hand circularly polarized light propagating in the $-Z$ direction, the $k = 1$, $q = 0$ component of the differential orientation cross section can be written as follows:[5c]

$$\sigma^{j}_{10}(\varphi,\vartheta) = \frac{3\sqrt{3}\sigma_0}{4\pi}\left[\alpha_1 \cos^2\vartheta + \frac{\gamma_1}{2}\sin^2\vartheta\right] \quad (28a)$$

$$\sigma_0 = \frac{4\pi^2\omega}{3c}[f_0(0,0) + 2f_0(1,1)]$$

The anisotropy parameters α_1 and γ_1 have clear physical meaning, being two different components of the standard photofragment orientation parameter under the condition of circularly polarized dissociation light. These parameters are related to the molecular frame components $j_{||}$ and $j_\perp$ of the total photofragment angular momentum j, respectively, while the component $j_{||}$ is parallel and the component $j_\perp$ is perpendicular to the recoil direction:

$$\alpha_1 = \frac{\langle (j_{||})_z \rangle}{\sqrt{j(j+1)}}; \quad \gamma_1 = \frac{\langle (j_\perp)_z \rangle}{\sqrt{j(j+1)}} \quad (28b)$$

where angle brackets mean averaging over the recoil angles φ, ϑ and the lower index Z corresponds to the Z projection of the vectors $j_{||}$ and $j_\perp$ in the laboratory frame.

Only the sum of the anisotropy parameters ($\alpha_1 + \gamma_1$) can be determined if the experimental procedure does not provide the selection of the photofragment orientation over the recoil directions. Both parameters α_1 and γ_1 can be either positive or negative. Their values are estimated below for the case when only one photofragment carries the angular momentum j different from zero and when the nonadiabatic interactions are negligible. The parameter α_1 has its extrema if perpendicular transitions dominate in the photoprocesses: $[\alpha_1]_{ext} = m/2[j(j+1)]^{1/2}$, where m is the quantum number of the photofragment magnetic sublevel populated in the photoprocesses. This parameter goes to zero for large j values; it is mainly responsible, for instance, for the results of the experiments.[9] The parameter γ_1 has its extrema when the parallel and perpendicular transitions are of the same intensity: $[\gamma_1]_{ext} = \pm 1/4$. It was shown in ref 19 that the coherent excitation of ICN molecules leads to strong orientation of CN fragments reported in ref 20. The third parameter γ_1' cannot be determined in the "parallel" experimental geometry described above (see Figure 1)[5c] but can be determined by measuring off-diagonal cross section elements (A_{11} or D_{11}) using probe light directed perpendicular to the Z axis.

Absorption (A_{10}) and dispersion (D_{10}) orientation cross sections calculated using (10), (11), (24), (25), and (28a) are shown in Figures 3 and 4 versus relative probe light frequency detuning x separately for each of the two terms in (28a). The contribution from the first (incoherent) term is given by curve 1, while the contribution due to the second (coherent) term is given by curve 2 in both figures. Similar relationships have recently been reported elsewhere.[13] It can be seen from Figures 3 and 4 that the relationships corresponding to the coherent and to the incoherent excitation of the molecules are quite different from each other, which gives the possibility to study they separately. The existence of two absorption maxima on the relationship 1 in Figure 3 and two dispersion contours on the relationship 1 in Figure 4 has a simple physical explanation: the photofragment angular distribution $\sim\cos^2\vartheta$ (28a) leads to production of two groups of the photofragments moving in opposite directions along the probe light beam (Z axis), which give their main contributions to the cross sections (10), (11) at two different frequency detunings.

3.4.3. Second-Order (Alignment) Cross Sections. In order to define alignment parameter, we first consider nonpolarized light propagating along the Z axis. Then using the results of

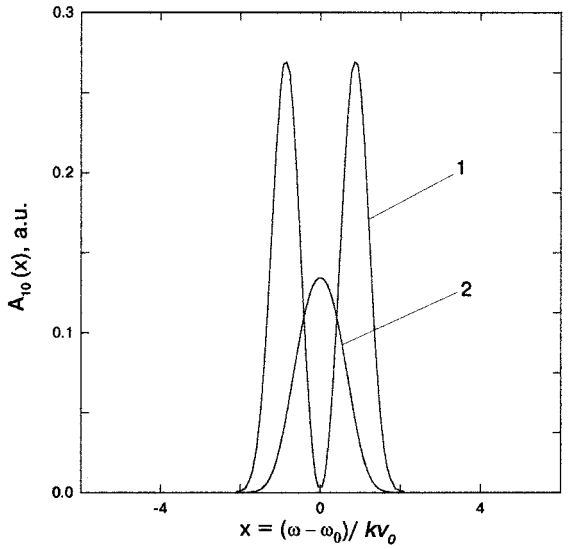

Figure 3. Absorption orientation cross sections A_{10} versus relative probe laser frequency detuning $x = (\omega - \omega_0)/kv_0$. The dissociation light is circularly polarized, and the photofragment total angular momentum is equal to $j = 1/2$. (1) Photofragments orientation produced via incoherent excitation of the molecule. The anisotropy parameter α_1 is equal to $1/(2\sqrt{3})$. (2) Photofragments orientation produced via coherent excitation of the molecule. The anisotropy parameter γ_1 is equal to $1/4$.

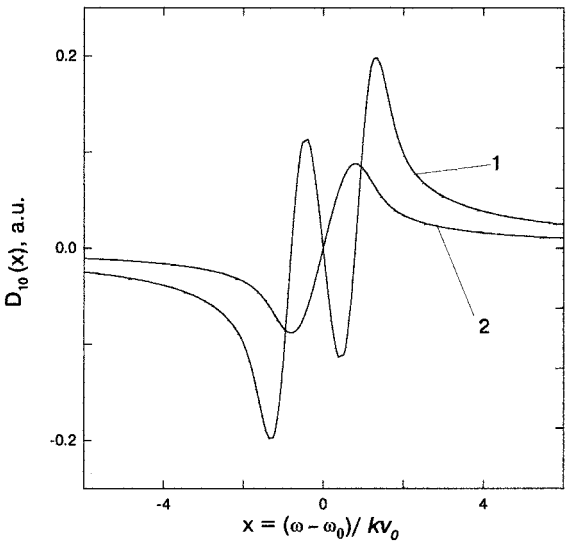

Figure 4. Dispersion orientation cross sections D_{10} versus relative probe laser frequency detuning $x = (\omega = \omega_0)/kv_0$. The dissociation light is circularly polarized. (1) Photofragments orientation produced via incoherent excitation of the molecule by circularly polarized light. (2) Photofragments orientation produced via coherent excitation of the molecule by circularly polarized light. The values of the anisotropy parameters α_1 and γ_1 are the same as in Figure 3.

ref 5c the diagonal cross section $\sigma^{j}_{20}(\varphi,\vartheta)$ can be presented as follows

$$\sigma^{j}_{20}(\varphi,\vartheta) = \frac{\sqrt{5}\sigma_0}{4\pi}V(j)\Big\{P_2(\cos\vartheta)[s_2 + \alpha_2 P_2(\cos\vartheta)] + \frac{3}{2}\gamma_2\sin^2\vartheta\cos^2\vartheta + \frac{3}{8}\eta_2\sin^4\vartheta\Big\} \quad (29)$$

where $$V(j) = 5\left[\frac{j(j+1)}{(2j+3)(2j-1)}\right]^{1/2}$$

The s_2, α_2, γ_2, and η_2 are angular independent alignment anisotropy parameters:

$$s_2 = V(j)^{-1}\frac{f_2(0,0) + 2f_2(1,1)}{f_0(0,0) + 2f_0(1,1)} \quad (30a)$$

$$\alpha_2 = V(j)^{-1}\frac{f_2(1,1) - f_2(0,0)}{f_0(0,0) + 2f_0(1,1)} \quad (30b)$$

$$\gamma_2 = 2\sqrt{3}V(j)^{-1}\frac{\mathrm{Re}[f_2(1,0)]}{f_0(0,0) + 2f_0(1,1)} \quad (30c)$$

$$\eta_2 = \sqrt{6}V(j)^{-1}\frac{f_2(1,-1)}{f_0(0,0) + 2f_0(1,1)} \quad (30d)$$

The anisotropy parameters s_2, α_2 describe the photofragment alignment produced by noncoherent optical transitions in the dissociating molecule. The parameter s_2 (30a) is responsible for the alignment component that does not depend on the angles φ, ϑ in the molecular frame and vanishes after averaging the photofragment alignment over the φ,ϑ. Besides, it is seen from (29) that this component gives contribution to the alignment angular distribution in the laboratory frame. The parameters α_2, γ_2, η_2 (28b,c,d) are responsible for the alignment components that depend on the angles φ, ϑ both in the molecular and in the laboratory frame. These parameters have clear physical meaning being components of standard diagonal alignment parameter[18] of the photofragments coming from three different dissociation mechanisms. These are incoherent perpendicular and parallel optical transition in the dissociating molecule (30b), coherent superposition of a parallel and a perpendicular transition (30c), and coherent superposition of two perpendicular transitions (30d), respectively. For instance,

$$\alpha_2 = \frac{\langle(3j_z^2 - j^2)_\alpha\rangle}{j(j+1)}$$

where angled brackets mean averaging over the recoil angles φ, ϑ. Only the sum of the anisotropy parameters ($\alpha_2 + \gamma_2 + \eta_2$) can be determined in a non-Doppler type experiment. The values of these parameters can be estimated for the case when only one photofragment carries the angular momentum j different from zero and the nonadiabatic interactions are negligible. These are $\alpha_2 = {}^1/_5$ for the parallel $\Sigma \rightarrow \Sigma$ transition in the molecule, $\alpha_2 = [3m^2 - j(j+1)]/10j(j+1)$, $\eta_2 = {}^3/_{10}$ for the perpendicular $\Sigma \rightarrow \Pi$ transition, and $\gamma_2 = 3/10[j(j+1)]^{1/2}$ for the same intensities of the parallel and perpendicular transitions. As shown in (10), (11), (19), and (21), both resonance and off-resonance alignment detection schemes where the probe light beam propagates along the Z axis lead to signals that depend on the real part of the alignment cross section Re-$[\sigma^j{}_{22}(\varphi,\vartheta)]$. Let the polarization vector of linearly polarized dissociation light be parallel to the Y axis of the laboratory frame and probe beam be parallel to the Z axis as shown in Figure 1c. Then using the results of ref 5c the cross section $\sigma^j{}_{22}(\varphi,\vartheta)$ can be presented as follows:

$$\sigma^j_{22}(\varphi,\vartheta) = \frac{\sqrt{30}\sigma_0}{16\pi}V(j)e^{2i\varphi}\Big\{\sin^2\vartheta[s_2 + \alpha_2[(1-\cos 2\varphi)P_2(\cos\vartheta) + \cos 2\varphi]] - \gamma_2\sin^2\vartheta[\cos^2\vartheta(1-\cos 2\varphi) + i\sin 2\varphi] + \frac{\eta_2}{4}[(1+\cos^2\vartheta)\sin^2\vartheta + (1+\cos^2\vartheta)^2\cos 2\varphi - 4i\cos^2\vartheta\sin 2\varphi]\Big\} \quad (31)$$

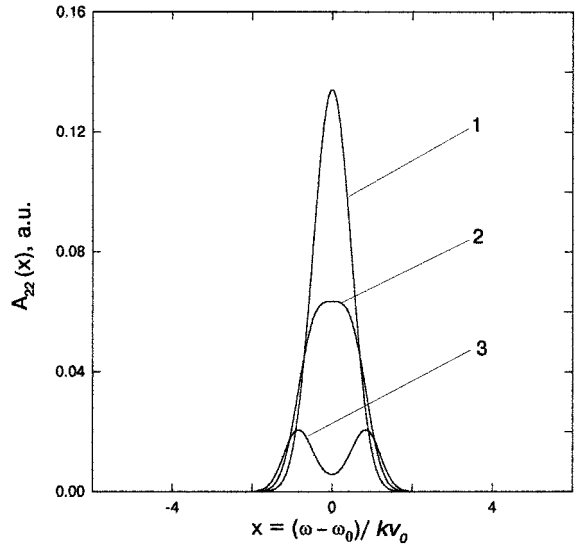

Figure 5. Absorption alignment cross sections Re[A_{22}] versus relative probe laser frequency detuning $x = (\omega - \omega_0)/k\upsilon_0$. The dissociation light is linearly polarized, and the photofragment total angular momentum is equal to $j = 1$. (1) Photofragments alignment produced via incoherent excitation of the molecule. The anisotropy parameter α_2 is equal to ${}^1/_5$. (2) Photofragments alignment produced via coherent superposition of a parallel and a perpendicular transition. The anisotropy parameter γ_2 is equal to $3/(10\sqrt{2})$. (3) Photofragments alignment produced via coherent superposition of two perpendicular transitions. The anisotropy parameter η_2 is equal to ${}^3/_{10}$.

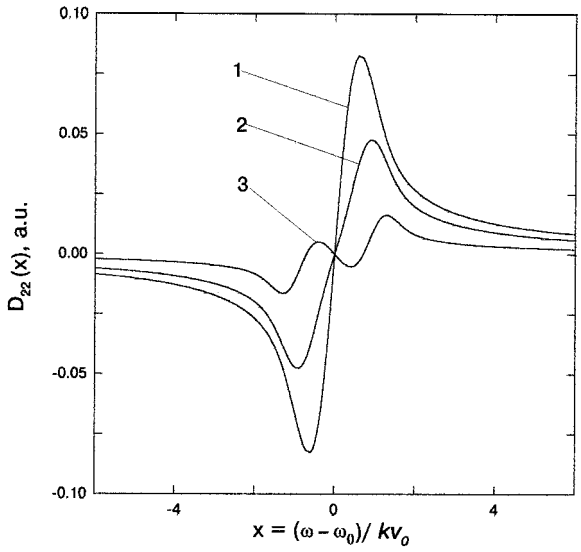

Figure 6. Dispersion orientation cross sections Re[D_{22}] versus relative probe laser frequency detuning $x = (\omega - \omega_0)/k\upsilon_0$. Dissociation light is linearly polarized, and the photofragment total angular momentum is equal to $j = 1$. (1) Photofragments alignment produced via incoherent excitation of the molecule. (2) Photofragments alignment produced via coherent superposition of a parallel and a perpendicular transition. (3) Photofragments alignment produced via coherent superposition of two perpendicular transitions. The anisotropy alignment parameters α_2, γ_2, and η_2 are the same as in Figure 5.

Absorption (Re[A_{22}]) and dispersion (Re[D_{22}]) alignment cross sections calculated using (10), (11), (24), (25), and (31) are shown in Figures 5 and 6 versus relative probe light frequency deturning x separately for each of the three terms in (29). The contribution from the first (incoherent) term is given by curve 1 while the contributions from two coherent terms are given by curves 2 and 3. Figures 5 and 6 show that all three anisotropy parameters in (30) can be determined in the described experimental scheme.

It should be noted however that the parameters in (30) do not give a full description of the dissociation dynamics responsible for photofragments alignment because there should be in principle two other parameters γ_2', η_2' related to imaginary parts of the dynamical functions $f_2(1,0)$ and $f_2(1,-1)$ (see (30c,d)), which do not appear in (31). The former parameters would arise if elliptically polarized dissociation light could discussed while the latter can be neglected for the processes of direct photodissociation because in this case the dynamical functions $f_2(1,-1)$ are shown to be real.[5c]

The results presented above show that in principle the paramagnetic Faraday rotation technique can provide the same information about photodissociation dynamics as the resonance dichroism technic. Besides, use of the paramagnetic Faraday rotation technique to study the photodissociation dynamics can be very hopeful from experimental point of view because the contribution from the photofragments orientation and alignment to the signal are usually a small fraction of the probe light total absorption by the photofragments.[3,9] Comparatively large absorption decreases the accuracy of the measurements and can easily break the conditions of thin optical layer that can complicate the interpretation of the experimental results. More, the saturation of the photofragment resonance optical transitions can be easily achieved under the conditions of the one-photon detection scheme that can complicate much the interpretation of the experimental results. It is seen from Figures 4−6 that extremum points of the dispersion signals are relatively far from resonance, which can increase the accuracy of the experiments and simplify their interpretation. In the following section the results of experimental studies of spin-oriented Rb atoms produced in photodissociation of RbI molecules by circularly polarized light are presented by both in-resonance and off-resonance schemes.

IV. Experimental Studies of Spin-Oriented Rb Atoms Produced in Photodissociation of RbI

The experiments were carried out in order to detect and study the polarized photofragments at the same experimental conditions alternatively with resonant and off-resonant detection schemes and to compare the obtained results with each other and with the theoretical predictions presented above.

We studied oriented ground state $5^2S_{1/2}$ Rb atomic photofragments in photodissociation of RbI at 266 nm in the following reaction where the iodine atoms produced in their metastable state:

$$RbI(^1\Sigma_{0^+}) + h\nu(266\text{ nm}) \rightarrow Rb(5\ ^2S_{1/2}) + I(5\ ^2P_{1/2}) \quad (32)$$

It is well-known[21,22] that covalent excited states of alkali halides, correlating with a ground state $^2S_{1/2}$ alkali atom and a ^2P_j halide atom, are typical example of Hund case *c* that is defined by a projection Ω of the total molecular angular momentum *J* on an internuclear axis and by symmetry quantum numbers $\sigma = \pm$ for $\Omega = 0\sigma$ terms. Figure 7 shows qualitatively X $^1\Sigma^+$ ionic ground state and the covalent excited states of the RbI molecule as well as dissociation and probe channels. The absorption spectrum of RbI in the 250−330 nm region consists of two bands relating to two possible photodissociation channels that lead to the following pairs of atoms: $Rb(5^2S_{1/2}) + I(5\ ^2P_{3/2})$ and $Rb(5\ ^2S_{1/2}) + I(5\ ^2P_{1/2})$.[22] In our experiments at 266 nm, only the second excited molecular state was populated from the ground state and the second pair of the atoms arises (32). In this photodissociation channel the electronic molecular energy levels are not split by the van der Waals interaction at large internuclear distances that can increase Coriolis type nonadiabatic coupling and interference effects in the decaying molecule.

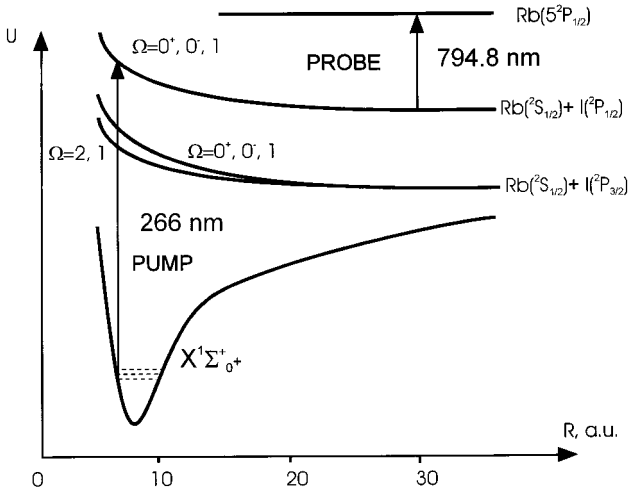

Figure 7. Potential curves of RbI molecule.[22]

4.1. Experimental Procedure. There are two optical transitions of different symmetry from the molecular ground state to the second excited state with approximately equal intensities: $X\ ^1\Sigma_0^+ \rightarrow 0^+$ and $X\ ^1\Sigma_0^+ \rightarrow 1$.[22] The value of anisotropy parameter β_0 reported by Su and Riley[23] is as follows: $\beta_0 = 0.54$. Spin-oriented ground state Rb atoms produced in the reaction (30) were already observed elsewhere[9c] when only the resonance detection technique was used.

In our experimental procedure and data analysis, we mainly followed the theoretical expressions (15), (16), (22), and (23) but there were also some important differences. Firstly, from the experimental point of view the direct following of (15) was not convenient because led to large experimental errors due to necessity of subtraction of two large values I_+ and I_- from each other. To avoid this problem, we combined pulsed dissociation light with continuous probe light and modulated the observed signals by applying an external magnetic field. This gave us a possibility to detect the difference (15) directly after each laser pulse. Secondly, in the interpretation of the experimental results presented below, we fixed the orientation signals by the intensity of the *absorbed* light given by the two last terms in (16) but not by the intensity of the *transmitted* light given by the whole expression. This approach was convenient because allowed us to determine the degree of orientation of the photofragments directly from the resonance experimental signals. We also used not only the collinear directions of the dissociation and probe light beams described in the section 3 but also another experimental geometry when the probe beam was perpendicular to the dissociation beam as shown in Figure 8.

The experimental procedure we used in principle allows us to extract all information about the photofragment orientation and alignment from the one-laser pulse with sensitivity that is comparable with that provided by the one-photon LIF technique. The procedure is shown in Figure 8 and is similar to that described elsewhere.[9c] An absorption quartz cell containing RbI vapors at a pressure of $10^{-2}-10^{-3}$ Torr was illuminated by pulsed circularly polarized laser radiation at 266 nm that propagated perpendicularly to the direction of the permanent magnetic field H = 50 A/m. The dissociation light was generated as the fourth harmonic of a Q-switched Nd:YAG laser at 1064 nm with a pulse duration of $\tau = 10$ ns and repetition rate of 10 Hz. The circular polarization of the dissociation light was produced by using a prism linear polarizer and a quartz quarter-wave plate that provide a polarization degree of about

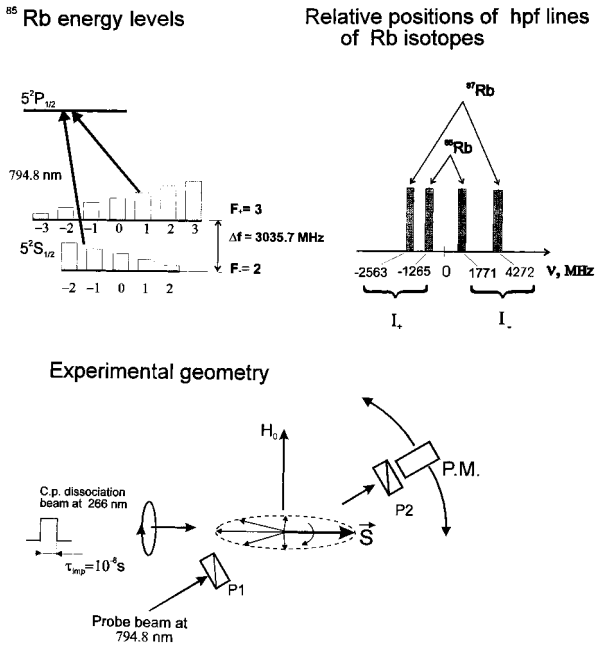

Figure 8. Experimental procedure.

95%. Purified isotopically reached $^{85}Rb^{127}I$ salt containing more that 90% of the ^{85}Rb isotope was used in the cell.

The mean angular momenta of the atoms processed around the magnetic field $\mathbf{H}_0$ as shown in Figure 8 caused oscillating optical circular dichroism/magnetic optical birefringence of the vapor for the probe light whose frequency was in the vicinity of the atomic absorption lines frequency. The optical circular dichroism/magnetic optical birefringence signal was detected by a probe resonance Rb D_1 line at 794.8 nm from an electrodeless radio frequency (rf) discharge rubidium lamp operating in a continuous regime. The probe beam propagated perpendicularly to the magnetic field $\mathbf{H}_0$, and its direction could be varied from antiparallel to perpendicular to the dissociation beam as shown in Figure 8. The probe beam passed successively through the polarizer P_1, the cell, and then the polarization analyzer P_2 onto a photodetector. In the case when the photofragments orientation was detected by the resonance circular dichroism technique, the same ^{85}Rb isotope was used both in the cell and in the rf discharge lamp, the initial probe light was unpolarized (no polarizer P_1 was used), and the analyzer P_2 was a circular one consisting of a mica quarter-wave plate and a linear dichroic polaroid. In the case when the photofragments orientation was detected by the paramagnetic Faraday rotation technique, the rf lamp contained the ^{87}Rb isotope while the cell contained the ^{85}Rb isotope, and both polarizer P_1 and analyser P_2 were linear dichroic polaroids with their axes directed 45° to each other. The hyperfine structure lines of ^{85}Rb and ^{87}Rb isotopes are known to be shifted from each other (see Figure 8), which provides a convenient way for the off-resonant detection of oriented Rb atoms.[11] The output from the photodetector was accumulated by a digital oscilloscope connected with a computer. The schematic setup is shown in Figure 9.

4.2. Experimental Results. Typical experimental signals corresponding to the off-resonance Faraday detection technique are shown in Figure 10, curves 1 and 2. The moment of the laser shot corresponds to the time $t = 0$. The signals are the average of the 20 laser pulses. The rapid decrease of the signal just after the laser shot is mainly a result of the probe light absorption by the Rb atoms produced in the cell. The main reason for this absorption was a partial overlap of the probe and absorption atomic lines. Then the absorption decreases

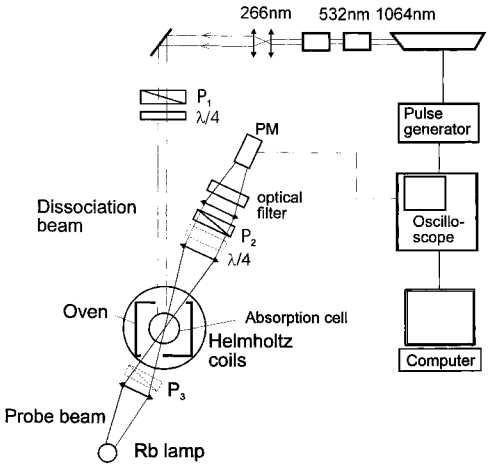

Figure 9. Experimental setup.

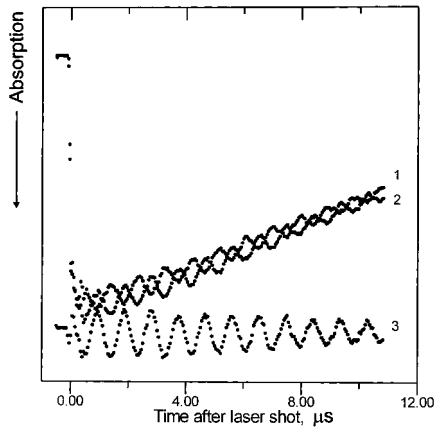

Figure 10. Typical experimental signals obtained by the Faraday detection technique. The signals 1 and 2 were obtained using the right- and left-hand circularly polarized dissociation light, respectively. The signal 3 (orientation signal) is the difference between the signals 1 and 2.

slowly due to the recombination of the atoms by collisions with the walls and with the molecules in the cell volume. There are dumping oscillations on the bottom of the signals that are caused by the free precession of the atomic angular momentum around the external magnetic field discussed above. The experimental signals obtained by the resonance detection technique were similar to those presented in Figure 10 (see ref 9c) but had a several times higher ratio between the population step and the oscillation amplitude. Moreover, the orientation signals obtained by the Faraday detection technique could be observed in the much larger pressure range of the molecular vapor than that by the dichroism detection technique.

Signals 1 and 2 in Figure 10 were obtained when the dissociation light was right and left-hand circular polarized, respectively. It can be seen from Figure 10 that the difference between the phases of these two signals is equal to π. Signal 3 in Figure 10 is the difference of signals 1 and 2. This signal has pure orientation nature as does not contain the "population step" that exists in signals 1 and 2. The orientation signal amplitude decreased with time mainly due to the depolarization collisions of the ground state Rb atoms with the RbI molecules in the cell volume. The orientation signals detected by both resonance and off-resonance techniques were fitted as follows

$$\frac{U_{or}(t)}{U_0} = A^{exp} \sin(\omega_0 t + \phi) \exp(-\gamma_0 t) \qquad (33)$$

where U_0 is the "population step", ω_0 is a precession frequency

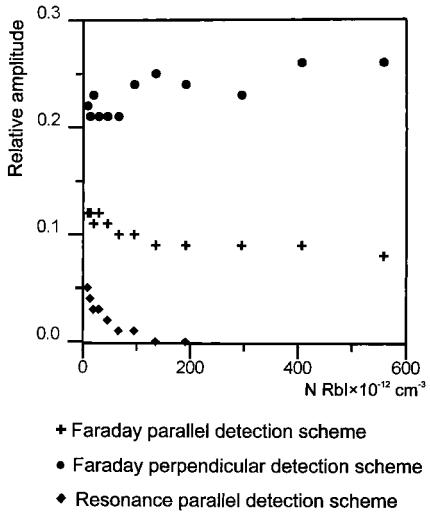

Figure 11. Amplitudes of the orientation signals obtained by using different detection techniques versus RbI concentration. The amplitudes are fixed by total absorption of the light by the photofragments.

of the ground state Rb hpf angular momenta around the external magnetic field $\mathbf{H}_0$, and the amplitude $A^{\exp}$, phase ϕ, and relaxation rate γ_0 are fitting parameters. Then the amplitudes $A^{\exp}$ was extrapolated to the zero-dissociation light intensity in order to eliminate the influence of the photofragment thick optical layer and molecular transition saturation effects on the measured atomic orientation.

The experiments were carried out in two different geometries when the probe light beam was either perpendicular or almost parallel to the dissociation laser beam. With both in-resonance and off-resonance detection techniques, the amplitudes of the orientation signals were found to depend on the relative direction of the probe beam compared to that of the dissociation beam. The experimental results presented in Figure 10 were observed when the probe beam passed through the cell perpendicularly to the dissociation beam. This geometry will be referred below as the perpendicular detection scheme. The orientation signals detected in this scheme were about two times larger than that detected in the parallel scheme when the probe beam was transmitted at a small angle (about 5°) toward the dissociation beam. The amplitudes of the orientation signals determined by the resonance technique behaved antipathetically relative to the amplitudes of the signals detected by the Faraday technique: the orientation signals detected in the parallel detection scheme were about three time larger than that in the perpendicular detection scheme.

The amplitudes of the orientation signals $A^{\exp}$ obtained by the Faraday and resonance detection techniques and normalized to the corresponding "population steps" are shown versus the RbI concentration in Figure 11. Curves 1 and 2 in this figure relate to the perpendicular and parallel Faraday detection schemes, respectively, while curve 3 corresponds to the resonance parallel detection scheme. Figure 11 evidently manifests the great advantage of using nonresonance schemes to detect photofragments orientation at relatively high molecular concentrations.

4.3. Discussion. The observed dependence of the orientation signal amplitude on the relatie directions of the probe and dissociation beams can be understood by taking into consideration the contributions to the signals of two rubidium hyperfine ground state energy levels. The quantum mechanical observables describing the orientation of the ground state Rb atoms are the components of mean total atomic angular momentum $\langle \mathbf{F} \rangle_{\pm} = \langle \mathbf{I} \rangle_{\pm} + \langle \mathbf{S} \rangle_{\pm}$ for upper ($\langle \rangle_+$) and lower ($\langle \rangle_-$) hpf sublevel, respectively. Here **S** and **I** are electronic and nuclear spin operators, $S = {}^1/_2$, and $F_{\pm} = I \pm {}^1/_2$, where $I = {}^5/_2$ is the nuclear spin. The initial hpf orientation vectors $\langle \mathbf{F} \rangle_+$ and $\langle \mathbf{F} \rangle_-$ of the Rb atoms just after the laser pulse were directed along the Z axis antiparallel to each other. The hyperfine g-factors related to the F_+ and F_- sublevels have the same values but opposite signs, and thus the orientation vectors $\langle \mathbf{F} \rangle_+$ and $\langle \mathbf{F} \rangle_-$ precessed around the external magnetic field $\mathbf{H}_0$ with the same frequency ω_0 but in opposite directions. The total orientation signal oscillated, while the orientation vectors $\langle \mathbf{F} \rangle_+$ and $\langle \mathbf{F} \rangle_-$ precessed around the magnetic field $\mathbf{H}_0$ having its extrema when the orientation vectors were directed along the probe beam. This signal was a sum of the signals from the $F_{\pm}$ hpf sublevels and depended on the selection rules for dipole optical transitions, on the directions of the $\langle \mathbf{F} \rangle_{\pm}$ orientation vectors, and on the intensities of the hpf components in the probe light atomic line. The expression describing the orientation signal amplitude A^{th} in the case of the resonance and off-resonance technique and for the parallel and perpendicular detection schemes can be obtained on the basis of (15), (16), (18), (22), and (23) and the transformation properties of rotation D-functions.[16] We assume that the hpf structure of the Rb(5^2P) excited states is unresolved and write expression for the amplitude of the orientation signal at the transitions $^2S_{1/2} \rightarrow {}^2P$ as follows:

$$\frac{A^{\text{th}}}{U_0} = \frac{11/4 - j_e(j_e+1)}{(I+1)J_+^A + I\,J_-^A}\left[\frac{(I+1)(2I+3)}{3(2I+1)}\,J_+^n \pm \frac{I(2I-1)}{3(2I+1)}\,J_-^n\right] P_e \exp(-\gamma_0 t) \quad (34)$$

where the upper and lower signs ($\pm$) relate to the parallel and perpendicular detection schemes, respectively, $I = {}^5/_2$ is a nuclear atomic spin; $P_e = \langle S_Z \rangle / S$ is an initial spin orientation degree of the $j_g = S = {}^1/_2$ atoms; $j_e = {}^1/_2$, ${}^3/_2$ are the total electronic angular momenta of the atomic ^{2}P excited state; J_+^n and J_-^n where $n =$ A, D are the functions introduced in (22) and (23) and written for the hpf components of the probe light line at the $F_+ \rightarrow j$ and $F_- \rightarrow j$ transitions, respectively. The orientation degree P_e used in (34) is proportional to the orientation parameter[4] as follows: $P_e = ((j+1)/j)^{1/2} O_1$.

In the case of the resonance detection technique the functions J_+^A, J_-^A in (34) are always positive, and therefore the orientation signal has its maximum for the parallel detection scheme when the hpf orientation vectors $\langle \mathbf{F} \rangle_+$ and $\langle \mathbf{F} \rangle_-$ are *antiparallel* to each other. The intensities of the hpt components of the probe line at 794.8 nm from the resonance rf lamp can be assumed to be approximately the same. Then for the case of the ^{85}Rb D_1 resonance line ($j_e = {}^1/_2$), (34) leads to the following ratio of the orientation signals in the perpendicular and parallel detection schemes: $[A(\text{perp})/A(\text{parall})]_{\text{theory}} \cong 9/19$. The experimentally observed ratio was found to be $[A(\text{perp})/A(\text{parall})]_{\text{exp}} = 0.3 \pm 0.2$, which is in agreement with the theoretical prediction within experimental errors.

In the case of the off-resonance detection technique the integrals J_+^D, J_-^D in (34) can be either positive or negative depending on the position of the probe light line relative to the center of the dispersion cross section profile (see Figure 4). It can be seen from Figures 4 and 8 that when the hpf structure lines of the ^{87}Rb isotope are used to detect the ^{85}Rb isotope photofragments the integrals J_+^D and J_-^D have opposite signs. Thus, according to the (33) the amplitude of the Faraday signal is larger in the perpendicular detection scheme and has its maximum when the hpf orientation vectors $\langle \mathbf{F} \rangle_+$ and $\langle \mathbf{F} \rangle_-$ are *parallel* to each other, which is in agreement with the observed experimental results.

The experimental signals detected in the present work by the resonance technique were similar to those reported elsewhere[9c] but have a better signal-to-noise ratio because the detection channel was improved. The initial spin orientation degree P_e was determined using the amplitude A^{exp} of the experimental orientation signal (33) and the theoretical expression (34). The initial spin orientation degree P_e of the Rb(5S) atoms produced in the dissociation reaction (32) was found to be $P_e = 0.11 \pm 0.02$. This value is about twice as small as our previous result for the same reaction $P_e = 0.20 \pm 0.02$ reported in ref 9c. This disagreement was found to be a result of a wrong fitting procedure under poor signal-to-noise conditions of the experiment.[9c]

It can be seen from (34) that the experimental results obtained by the Faraday detection technique and presented in Figure 11 cannot be used alone to determine the photofragment orientation degree P_e because the normalization factor U_0 for this procedure should be taken from the resonance detection measurement. The conditions of our experiment were not favorable for such complex measurements because the probe light discharge Rb lamps we used had different spectral characteristics. Therefore we did not measure the photofragment orientation degree for the Faraday technique signals.

The orientation degree of the Rb photofragments P_e is the only parameter in (34) containing the information about photodissociation dynamics. The experiment described above was not of the Doppler spectroscopy type. Thus the orientation degree determined in the present work is proportional to the sum of the orientation anisotropy parameters $P_e = \sqrt{3}\,(\alpha_1 + \gamma_1)$ (see (27a,b)) extrapolated to the moment of the laser pulse. The Doppler spectroscopy type experiments are now in progress in our laboratory and will be used to determine the parameters α_1 and γ_1 separately.

V. Conclusion

This paper presents the results of theoretical and experimental studies of two different detection techniques that were used to investigate the angular momentum anisotropy distributions of the photofragments produced in molecular photodissociation: the magnetic dichroism and magnetic birefringence techniques. The frame independent tensor form of the general expression describing the difference between the initial and the final polarization matrix of the probe light beam passing through the photofragment vapor is presented.

The procedures of detection of the photofragment angular momentum anisotropy distribution by each of the techniques are compared and discussed. Three orientation and five alignment anisotropy parameters are presented that can be determined from these studies. It is shown that in principle each of the techniques can give the same information about the photodissociation dynamics; besides, the birefringence technique has certain experimental advantage allowing a reduction of the influence of isotropic absorption of the probe beam and a decrease of the saturation effects.

Experiments have been carried out to study the spin orientation of ground state Rb atoms produced in photodissociation of RbI at 266 nm by each of the techniques. The experimental results show that the off-resonance birefringence technique allows detection of the photofragment orientation in a much wider concentration region of the parent molecules and with a better signal-to-noise ratio. The contribution from the orientated Rb hpf energy states to the observed signals were studied and treated theoretically. The initial degree of electron spin orientation of the Rb atoms produced in the reaction was found to be $P_e = 0.11 \pm 0.02$, which is an improvement to the result published elsewhere.[9c]

TABLE A1: Bipolar Moments in Terms of the Anisotropy Parameters. The Dissociation Light Is Linearly Polarized along the Laboratory *Z* Axis[a]

bipolar moment	expression
$b_0^0(0,0)$	1
$b_0^2(0,2)$	$\frac{1}{5}\beta_0$
$b_0^0(2,2)$	$\frac{V(j)}{\sqrt{5}}s_2$
$b_0^2(2,0)$	$-\frac{2V(j)}{5}[\alpha_2 + \gamma_2 + \eta_2]$
$b_0^2(2,2)$	$\frac{2\sqrt{2}V(j)}{5\sqrt{7}}\left[\alpha_2 + \frac{\gamma}{2} - \eta_2\right]$
$b_0^2(2,4)$	$-\frac{2\sqrt{2}V(j)}{5\sqrt{7}}\left[\alpha_2 - \frac{4\gamma}{3} + \frac{1}{6}\eta_2\right]$
$b_0^2(1,2)$	$-\frac{2\sqrt{6}}{5}i\gamma_1'$

[a] The photofragment angular momentum dependent coefficient $V(j)$ is given in the (29). Note that the expression presented in the last row corresponds to the effect of the photofragment orientation by linearly polarized light.[5c]

Acknowledgment. The authors are much grateful to A. G. Suits and A. S. Bracker for fruitful discussions. The research described in this publication was made possible by Grant INTAS-93-1809-ext and CRDF Grant N RP1-223.

Appendix: Relationship between the Anisotropy Parameters and the Bipolar Moments

The general relationship between the semiclassical bipolar moments[5a] and the dynamical functions is given in expression B6 of ref 5c. This relationship depends not only on the photodissociation dynamics but also on the polarization of the dissociation light. Here we restrict ourselves to three lowest photofragment polarization momenta $k = 0, 1, 2$ and describe the case of linearly polarized light with the polarization vector along the space-fixed Z axis. After renormalization of expression B6 from ref 5c in order to satisfy the condition $b_0^0(0,0) = 1$, the nonzero bipolar moments in terms of the anisotropy parameters (27) and (30) are presented in the Table A1.

References and Notes

(1) (a) Zare, R. N.; Herschbach, D. R. *Proc. IEEE* **1963**, *51*, 173. (b) Ling, J. H.; Wilson, K. R. *J. Chem. Phys.* **1976**, *65*, 881. (c) Green, C. H.; Zare, R. N. *Annu. Rev. Phys. Chem.* **1982**, *33*, 119. (d) Simons, J. P. *J. Phys. Chem.* **1987**, *91*, 5378. (e) Houston, P. L. *J. Phys. Chem.* **1987**, *91*, 5388. (f) Hall, R. E.; Sivakumar, N.; Chawia, D.; Houston, P. L. *J. Chem. Phys.* **1988**, *88*, 3682. (g) Ashold, M. N. R.; Lambert, I. R.; Mordaunt, D. H.; Morley, G. P.; Vestern, C. M. *J. Phys. Chem.* **1982**, *96*, 2938. (h) North, S. W.; Hall, G. E. *J. Phys. Chem.* **1996**, *104*, 1864.

(2) (a) Busch, G. E.; Mononey, R. T.; Morse, R. I.; Wilson, K. R. *J. Chem. Phys.* **1969**, *51*, 837. (b) Zare, R. N. *Mol. Photochem.* **1972**, *4*, 1. (c) Busch, G. E.; Wilson, K. R. *J. Chem. Phys.* **1972**, *56*, 3626. (d) Simons, J. P. *Gas Kinetics and Energy Transfer*; Specialists Periodic Reports 2; Chemical Society: London, 1977; p 58.

(3) (a) Van Brunt, R. J.; Zare, R. N. *J. Chem. Phys.* **1968**, *48*, 4304. (b) Rothe, E. W.; Krause, U.; Düren, R. *Chem. Phys. Lett.* **1980**, *72*, 100. (c) Vasyutinskii, O. S. *JETP Lett.* **1980**, *31*, 428; *Sov. Phys. JETP* **1981**, *54*, 855. (d) Vigué, J.; Grangier, P.; Roger, G.; Aspect, A. *J. Phys. Lett. (Paris)* **1981**, *42*, L531. (e) Vigué, J.; Beswick, J. A.; Broyer, M. *J. Phys. (Paris)* **1983**, *44*, 1225. (f) Kato, H.; Onomichi, K. *J. Chem. Phys.* **1985**, *82*, 1642. (g) Kato, H. *Faraday Discuss. Chem. Soc.* **1986**, *82*, 1. (h) Zafiropulos, V.; Kleiber, P. D.; Sando, K. M.; Zeng, X.; Lyyra, A. M.; Stwalley, W. C. *Phys. Rev. Lett.* **1988**, *61*, 1485. (i) Kleiber, P. D.; Wang, J.-X.; Sando, K. M.; Zafiropulos, V.; Stwalley, W. C. *J. Chem. Phys.* **1991**, *95*, 4168.

(4) (a) Blum, K. *Density Matrix Theory and Applications*, 2nd ed.; Plenum: New York, 1966. (b) Zare, R. N. *Angular Momentum*; Wiley: New York, 1988.

(5) (a) Dixon, R. N. *J. Chem. Phys.* **1986**, *85*, 1866. (b) Hall, G. E.; Sivakumar; Houston, P. L.; Burak, I. *Phys. Rev. Lett.* **1986**, *56*, 1671. (c) Siebbeles, L. D. A.; Glass-Maujean, M.; Vasyutinskii, O. S.; Beswick, J. A.; Roncero, O. *J. Chem. Phys.* **1994**, *100*, 3610. (d) Vasyutinskii, O. S. *Opt. Spectrosc.* **1983**, *54*, 524. (e) Wang, Y.; Loock, H. P.; Cao, J.; Qian, C. X. W. *J. Chem. Phys.* **1985**, *102*, 808. (f) Mo, Y.; Katayanagi, H.; Heaven, M. C.; Suzuki, T. *Phys. Rev. Lett.* **1996**, *77*, 830. (g) Suzuki, T.; Katayanagi, H.; Mo, Y.; Tonokura, K. *Chem. Phys. Lett.* **1996**, *256*, 90.

(6) (a) Band, Y. B.; Freed, K. F.; Singer, S. J. *J. Chem. Phys.* **1983**, *72*, 6060; **1986**, *84*, 3762; **1987**, *86*, 1650. (b) Glass-Maujean, M.; Beswick, J. A. *Phys. Rev. A.* **1987**, *36*, 1170; **1988**, *38*, 5560. (c) Dubs, R. L.; Julienne, P. S. *J. Chem. Phys.* **1991**, *95*, 1977. (d) Vasyutinskii, O. S. *Khim. Fiz.* (USSR) **1986**, *5*, 768. (e) Kupriyanov, D. V.; Vasyutinskii, O. S. *Chem. Phys.* **1993**, *171*, 25.

(7) (a) Case, D. A.; McClelland, G. M.; Herschbach, D. R. *Mol. Phys.* **1978**, *35*, 541. (b) Green, C. H.; Zare, R. N. *J. Chem. Phys.* **1983**, *78*, 6741. (c) Rowe, M. D.; McCaffery, A. J. *Chem. Phys.* **1979**, *43*, 35. (d) Bain, A. J.; McCaffery, A. J. *J. Chem. Phys.* **1984**, *80*, 5882. (e) Kummel, A. C.; Sitz, G. O.; Zare, R. N. *J. Chem. Phys.* **1986**, *85*, 6874. *Ibid* **1988**, *88*, 6707. (f) Umeba, R.; Hinchliffe, R. D.; Cline, J. I. *J. Chem. Phys.* **1995**, *103*, 7934.

(8) (a) Chandler, D. W.; Houston, P. L. *J. Chem. Phys.* **1987**, *87*, 1445. (b) Chandler, D. W.; Thoman, J. W.; Sitz, G. O.; Janssen, M. H. M.; Stolte, S.; Parker, D. H. *J. Chem. Soc., Faraday Trans.* **1989**, *85*, 1305. (c) Chandler, D. W.; Janssen, M. H. M.; Stolte, S.; Strickland, R. N.; Thoman, J. W.; Parker, D. H. *J. Phys. Chem.* **1990**, *94*, 4839. (d) Suits, A. G.; Bontuyan, L. S.; Houston, P. L.; Whitaker, B. J. *J. Chem. Phys.* **1992**, *96*, 8618. (e) Suits, A. G.; Miller, R. L.; Bontuyan, L. S.; Houston, P. L. *J. Chem. Soc., Farady Trans.* **1993**, *89*, 1443. (f) Suzuki, T.; Hradil, V. P.; Hewitt, S. A.; Houston, P. L.; Whitaker, B. J. *Chem. Phys. Lett.* **1991**, *187*, 257.

(9) (a) Kupriyanov, D. V.; Sevastianov, B. N.; Vasyutinskii, O. S. *Z. Phys. D: At., Mol. Clusters* **1990**, *15*, 105. (b) Evseev, A. G.; Kupriyanov, D. V.; Picheyev, B. V.; Sevastianov, B. N.; Vasyutinskii, O. S. *Chem. Phys.* **1993**, *171*, 45. (c) Kupriyanov, D. V.; Picheyev, B. V.; Vasyutinski, O. S. *J. Phys. B: At., Mol. Opt. Phys.* **1993**, *26*, L803.

(10) Kastler, A. *Compt. Rend.* **1951**, *232*, 953.

(11) Happer, W. *Rev. Mod. Phys.* **1972**, *44*, 169.

(12) Cohen-Tannoudji, C.; Laloë, F. *J. Phys. (Paris)* **1967**, *28*, 505, 722.

(13) Kupriyanov, D. V.; Sokolov, I. M.; Subbotin, S. V. *Opt. Spectrosc.* **1996**, *80*, 728.

(14) Demtröder, W. *Laser Spectroscopy*, 2nd ed.; Springer-Verlag: Berlin, Heidelberg, 1996.

(15) Landay, L. D.; Lifshitz, E. M. *Field Theory*; Peace: Moscow, 1962.

(16) Varshalovich, D. A.; Moskalev, A. N.; Khersonskii, V. K. *Quantum theory of angular momentum*; World Scientific: Singapore, 1988.

(17) Alexandrov, E. B.; Chaika, M. P.; Khvostenko, G. I. *Interference of atomic states*; Springer: Berlin, 1993.

(18) Fano, U.; Macek, J. H. *Rev. Mod. Phys.* **1973**, *45*, 553.

(19) (a) Vigué, J.; Girard, B.; Gouwdard, G.; Billy, N. *Phys. Rev. Lett.* **1989**, *62*, 1358. (b) Beswick, J. A.; Glass-Maujean, M.; Roncero, O. *J. Chem. Phys.* **1992**, *96*, 7514.

(20) (a) Hasselbrink, E.; Waldeck, J. R.; Zare, R. N. *Chem. Phys.* **1988**, *126*, 191. (b) Black, J. F.; Hasselbrink, E.; Waldeck, J. R.; Zare, R. N. *Mol. Phys.* **1990**, *71*, 1143.

(21) Mulliken, R. S. *Phys. Rev.* **1937**, *51*, 310.

(22) Davidovits, P.; McFadden, D. L. *Alkali Halide Vapours*; Academic: New York, 1979.

(23) Su Tzu-min R.; Riley, S. J. *J. Chem. Phys.* **1979**, *71*, 3194.